Heliyon 8 (2022) e11752

Contents lists available at ScienceDirect

Heliyon

journal homepage: www.cell.com/heliyon

Research article

Electromagnetically induced absorption in Rb atoms with circular polarization of laser beams: Effects of neighboring transitions

Zeeshan Ali Safdar Jadoon [a], Aisar Ul Hassan [a], Heung-Ryoul Noh [b,*], Jin-Tae Kim [a,*]

[a] Department of Photonic Engineering, Chosun University, Gwangju 61452, Republic of Korea
[b] Department of Physics, Chonnam National University, Gwangju 61186, Republic of Korea

ARTICLE INFO

Keywords:
Electromagnetically induced absorption
Electromagnetically induced transparency
Rubidium

ABSTRACT

We have studied the effects of neighboring transitions on electromagnetically induced absorption (EIA) and electromagnetically induced transparency (EIT) in the D2 transition line in Rb atoms with respect to the same circular polarization configurations ($\sigma^+ - \sigma^+$) of coupling and probe lasers. Spectra for the open $F_g = 2 \rightarrow F_e = 2$ transition of ^{87}Rb and the $F_g = 3 \rightarrow F_e = 2$ and 3 transitions of ^{85}Rb exhibit EIA, resulting from the neighboring effect of $F_g = 2 \rightarrow F_e = 3$ and $F_g = 3 \rightarrow F_e = 4$ transitions, respectively. In contrast, EIT is observed for the open $F_g = 2 \rightarrow F_e = 1$ transition of ^{87}Rb, which indicates greater hyperfine energy splittings of ^{87}Rb and weaker neighboring effects than those of ^{85}Rb. Based on the theoretical results, we can confirm that EIT in the case of $F_g > F_e$ for ^{87}Rb for the same circular polarization configuration transforms into EIA due to the magnitude of the neighboring effects with a decrease in the hyperfine energy splittings.

1. Introduction

Since the discovery of electromagnetically induced absorption (EIA) and electromagnetically induced transparency (EIT) in the 1990s, various studies using Hanle [1, 2, 3, 4, 5, 6, 7, 8] and coupling-probe configurations [9, 10, 11, 12] have been performed. However, novel neighboring state effects have not been investigated extensively. These effects could govern unexpected EIA or EIT as we describe below.

Unresolved atomic systems under Doppler broadening effects present significant differences in observed EIA and EIT spectra due to the neighboring state contributions in a degenerate multilevel system [13]. In [13], we experimentally and theoretically confirmed that among the adjacent hyperfine transitions, the dominant cycling transition amplitude governs the observed spectral shapes at ^{85}Rb D2 transitions in a linear orthogonal polarization configuration. In a linear parallel polarization configuration of coupling and probe lasers, even in the case of the closed system of $F_g = 3 \rightarrow F_e = 4$ of ^{85}Rb, EIT was observed instead of EIA due to the neighboring effect of the dominant $F_g = 3 \rightarrow F_e = 3$ transition in the low-power regime [14].

In this work, EIA and EIT at $F_g = 2 \rightarrow F_e = 1, 2$ and 3 of ^{87}Rb and $F_g = 3 \rightarrow F_e = 2$, 3, and 4 of ^{85}Rb D2 transitions, as shown in Fig. 1(a) and (b) with relevant atomic energy level diagrams of ^{87}Rb and ^{85}Rb D2 transition line, respectively are investigated to understand the mechanisms of neighboring effects with the same circular polarization configuration ($\sigma^+ - \sigma^+$) of coupling and probe lasers. EIAs at all transitions of $F_g = 2 \rightarrow F_e = 2$, 3 of ^{87}Rb and $F_g = 3 \rightarrow F_e = 2$, 3, and 4 of ^{85}Rb D2 lines are observed. However, only the $F_g = 2 \rightarrow F_e = 1$ transition of ^{87}Rb transforms to EIT instead of EIA when the same circular polarizations of coupling and probe laser beams are used.

We realize that such differences result from different hyperfine energy splittings of ^{85}Rb and ^{87}Rb. We theoretically confirm that EIT for the $F_g = 2 \rightarrow F_e = 1$ transition of ^{87}Rb under the same circular polarization configuration transforms into EIA for the $F_g = 3 \rightarrow F_e = 2$ transition of ^{85}Rb owing to the increase in the neighboring effects with a decrease in the hyperfine energy splittings.

The simulated absorption profile considering the neighboring effect matches well with the experimental results. Coupling and probe fields produced by a single laser, combined with two acousto-optic modulators (AOMs) in a coupling-probe configuration, are used to experimentally investigate the effects on EIA (EIT) resonances in a weak coupling-probe power regime.

2. Theoretical calculation

EIA spectra were simulated via the same method used in our previous study [13] for the relevant atomic energy level diagrams shown in

* Corresponding authors.
E-mail addresses: hrnoh@chonnam.ac.kr (H.-R. Noh), kimjt@chosun.ac.kr (J.-T. Kim).

https://doi.org/10.1016/j.heliyon.2022.e11752
Received 20 August 2022; Received in revised form 11 October 2022; Accepted 14 November 2022

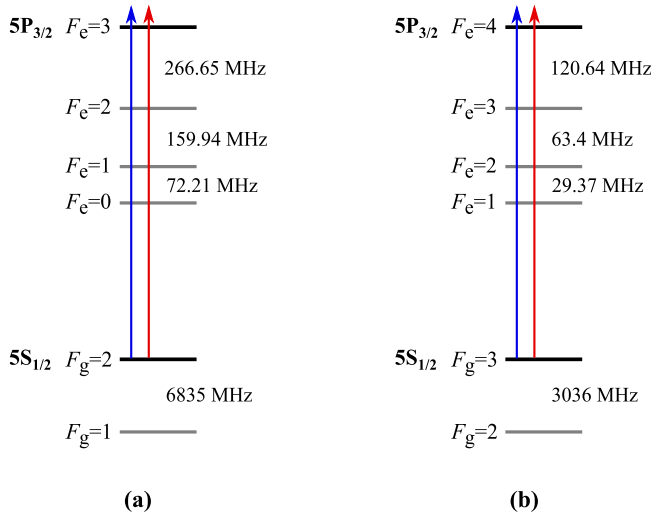

Fig. 1. Relevant atomic hyperfine energy level diagrams of (a) ^{87}Rb and (b) ^{85}Rb D2 transition lines, where the blue and red lines indicate the transitions by the coupling and probe beams, respectively.

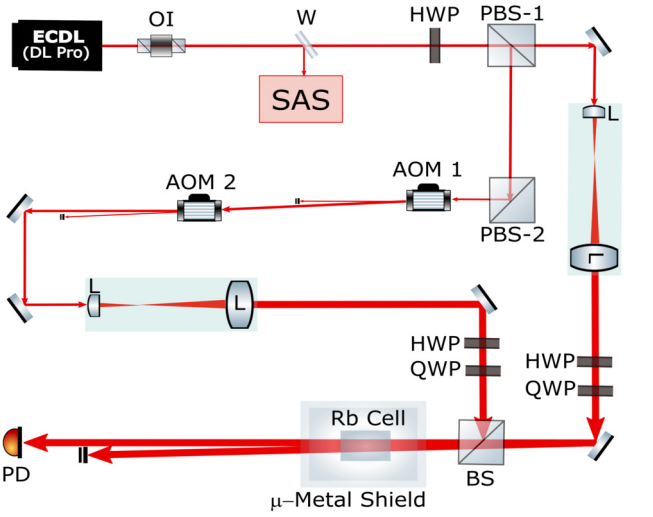

Fig. 2. Schematic of the experimental setup. Component symbols: OI: optical isolator; W: window; SAS: saturation absorption spectroscopy; HWP: half-wave plate; PBS: polarizing beam splitter; QWP: quarter-wave plate; L: lens; PD: photodiode; AOM: acousto-optic modulator.

Fig. 1(a) and (b). The only difference between this study and Ref. [13] was the polarization configuration: instead of an orthogonal linear polarization, the same circular polarization configuration ($\sigma^+ - \sigma^+$) of coupling and probe lasers was investigated. Here, we describe the method of calculation for ^{87}Rb briefly. The calculation for ^{85}Rb can be performed in an analogous method.

The density matrix equation governing the internal dynamics of the atom is given by

$$\dot{\rho} = -(i/\hbar)\left[H_0 + V, \rho\right] + \dot{\rho}_{\text{relax}}, \tag{1}$$

where the atomic (H_0) and interaction (V) Hamiltonians are given

$$\begin{aligned} H_0 = &-\sum_{m=-3}^{3} \hbar\delta_c \left|F_e = 3, m\right\rangle \left\langle F_e = 3, m\right| \\ &- \sum_{m=-2}^{2} \hbar\left(\delta_c + \Delta_{32}\right) \left|F_e = 2, m\right\rangle \left\langle F_e = 2, m\right| \\ &- \sum_{m=-1}^{1} \hbar\left(\delta_c + \Delta_{31}\right) \left|F_e = 1, m\right\rangle \left\langle F_e = 1, m\right|, \end{aligned} \tag{2}$$

$$\begin{aligned} V = &\frac{\hbar}{2} \sum_{F_e=1}^{3} \sum_{m=-2}^{2} \left(\Omega_c + \Omega_p e^{-i\delta_d t}\right) C_{2,m}^{F_e,m+1} \\ &\times \left|F_e, m+1\right\rangle \left\langle F_g = 2, m\right| + \text{h.c.}, \end{aligned} \tag{3}$$

respectively. In Eq. (1), $\dot{\rho}_{\text{relax}}$ represents the relaxation terms owing to the spontaneous emission and transit time decay, and is defined in Eq. (18) of Ref. [15]. In Eq. (2), $\delta_c (\equiv d_c - kv)$ is the effective detuning of the coupling beam where d_c denotes the detuning of the coupling beam, $k (= 2\pi/\lambda)$ is the wave vector, λ is the resonance wavelength of the laser, and v is the velocity of the atom. Δ_{32} (Δ_{31}) is the frequency spacing between the hyperfine states $\left|F_e = 3\right\rangle$ and $\left|F_e = 2(1)\right\rangle$. In Eq. (3), Ω_c (Ω_p) is the Rabi frequency of the coupling (probe) beam, $C_{F_g,m_g}^{F_e,m_e}$ is the normalized transition strength between $\left|F_e, m_e\right\rangle$ and $\left|F_g, m_g\right\rangle$ [15, 16], and h.c. denotes the Hermitian conjugate. $\delta_d (= \delta_p - \delta_c)$ is the effective frequency of the probe beam relative to the frequency of the coupling beam, and $\delta_p (\equiv d_p - kv)$ is the effective detuning of the probe beam where d_p denotes the detuning of the probe beam.

As reported in Ref. [13], the Zeeman coherences vanish. In addition, the populations are decomposed as $p_j = p_j^{(1)} + p_j^{(2)} e^{-i\delta_d t} + p_j^{(2)^*} e^{i\delta_d t}$ where j runs for all the magnetic sublevels [17]. The optical coherences between the sublevels with $m_e - m_g = 1$ are decomposed as follows [17, 18]:

$$\rho_{e_{m+1}^{F_e}, g_m} = \rho^{(1)}_{e_{m+1}^{F_e}, g_m} + \rho^{(2)}_{e_{m+1}^{F_e}, g_m} e^{-i\delta_d t} + \rho^{(3)}_{e_{m+1}^{F_e}, g_m} e^{i\delta_d t} + \rho^{(4)}_{e_{m+1}^{F_e}, g_m} e^{-2i\delta_d t},$$

where $\rho_{e_{m+1}^{F_e}, g_m} \equiv \left\langle F_e, m+1\right| \rho \left|F_g = 2, m\right\rangle$. The absorption coefficient of the probe beam is given by

$$\alpha = -\frac{3\lambda^2}{2\pi} \frac{N_{\text{at}}\Gamma}{\Omega_p} \int_{-\infty}^{\infty} dv \frac{e^{-(v/u)^2}}{\sqrt{\pi}u} \text{Im}\left[\sum_{F_e=1}^{3} \sum_{m=-2}^{2} C_{2,m}^{F_e,m+1} \rho^{(2)}_{e_{m+1}^{F_e}, g_m}\right],$$

where Γ is the decay rate of the excited, N_{at} is the atomic number density, and u is the most probable speed in the vapor cell.

3. Experimental methods

The experimental setup is shown in Fig. 2. A beam from a single tunable external cavity diode laser (DLPro, Toptica Inc.) with the wavelength of 780 nm is separated by a polarizing beam splitter (PBS). The probe beam and the pump beam were generated from a single laser with two AOMs. A half-wave plate (HWP) in front of the PBS controlled the beam powers of coupling and probe beams. The powers of the probe and coupling beams were 15 μW and 50 μW, respectively. The BS is used to overlap the co-propagating coupling and probe beams inside a vapor cell. A HWP in front of the PBS controlled the beam powers of coupling and probe beams. The powers of the probe and coupling beams were 15 μW and 50 μW, respectively.

The scanning of the coupling beam was scanned by transmitting the beam through two AOMs in a single-pass configuration. The modulation frequency for one of AOMs was fixed at 80 MHz and the other was scanned by ±1 MHz at the center of −80 MHz. We used Tektronix RF spectrum analyzer to calibrate the time axis (frequency) of the oscilloscope. The reason why coupling beam was scanned is to remove the Doppler broadening. It is worth noting that the spectra with the scanning of coupling detuning and probe detuning exhibit no discernable difference except for the existence of Doppler background in the probe detuning scanning case [19]. This is because EIT and EIA are coherent phenomena. Both the initial coupling and probe beams were expanded five times to have homogeneous beam of a diameter of 4 mm. A beam splitter was used to overlap the co-propagating coupling and probe beams inside a vapor cell. A vapor cell with the length and a diameter of 5 cm and 2.5 cm, respectively was shielded with five layers of μ-metal sheets that prevented stray and the Earth's magnetic fields from affecting the inside of the cell. The stray magnetic field was ap-

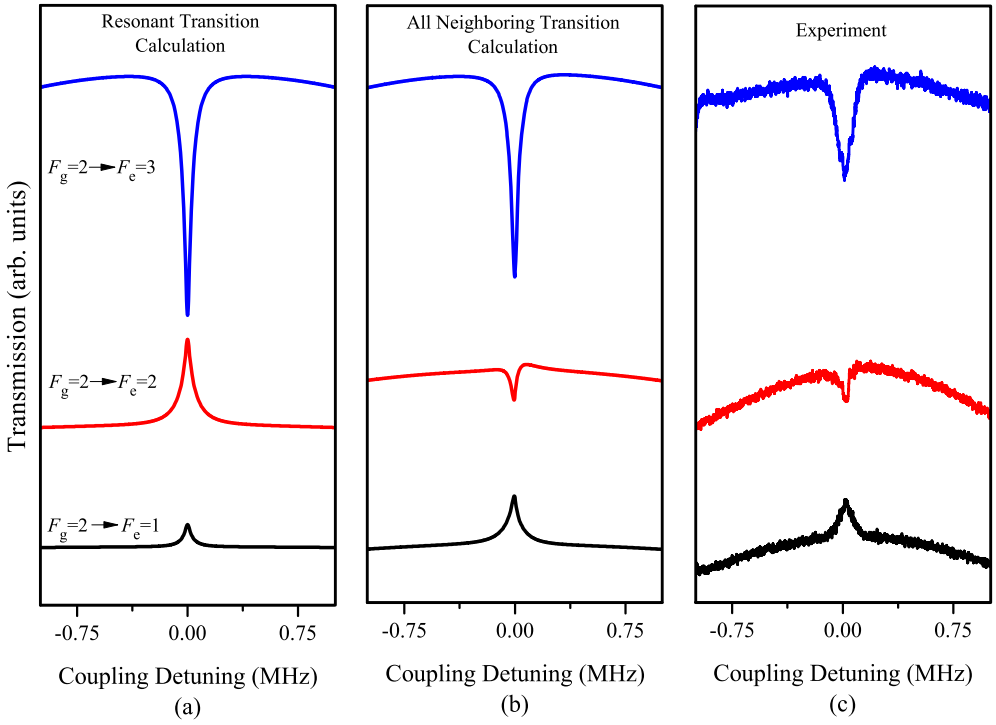

Fig. 3. Comparison of simulated and observed spectra at $F_g = 2 \rightarrow F_e = 1$, 2, and 3 of ^{87}Rb D2 line considering (a) DTLS with resonant transitions of only $F_g = 2 \rightarrow F_e = 1$, $F_g = 2 \rightarrow F_e = 2$, and $F_g = 2 \rightarrow F_e = 3$ shown vertically in (a); (b) all neighboring hyperfine transitions near the resonant (neighboring) transitions of $F_g = 2 \rightarrow F_e = 1$ (2 and 3), $F_g = 2 \rightarrow F_e = 2$ (1 and 3), and $F_g = 2 \rightarrow F_e = 3$ (1 and 2); and (c) experimentally observed spectra for the resonant transitions of $F_g = 2 \rightarrow F_e = 1$, $F_g = 2 \rightarrow F_e = 2$, and $F_g = 2 \rightarrow F_e = 3$.

proximately several mG, which may not cause significant variation in the EIT and EIA spectra [9].

4. Results and discussion

Spectrally resolved groups of the $F_g = 2 \rightarrow F_e = 1$, 2, and 3 transitions of ^{87}Rb and $F_g = 3 \rightarrow F_e = 2$, 3, and 4 transitions of ^{85}Rb were observed and simulated with respect to circular polarizations of probe and coupling fields in the low power regime. The results were analyzed based on the $\sigma^+ - \sigma^+$ polarization configuration for the ^{87}Rb and ^{85}Rb D2 lines and are shown in Figs. 3 and 4, respectively. Because we concentrated on the conversion between EIA and EIT which can be observed efficiently at the weak intensity of the coupling beam, we performed experiments and calculations in the low power regime.

A comparison of the simulated and observed spectra of the ^{87}Rb D2 line is shown in Fig. 3 considering (a) degenerate two-level system (DTLS) with resonant transitions of $F_g = 2 \rightarrow F_e = 1$, $F_g = 2 \rightarrow F_e = 2$, and $F_g = 2 \rightarrow F_e = 3$; (b) resonant transition of $F_g = 2 \rightarrow F_e = 1$ with neighboring hyperfine transitions of $F_g = 2 \rightarrow F_e = 2$ and 3, resonant transition of $F_g = 2 \rightarrow F_e = 2$ with neighboring transitions of $F_g = 2 \rightarrow F_e = 1$ and 3, resonant transition of $F_g = 2 \rightarrow F_e = 3$ with neighboring transitions of $F_g = 2 \rightarrow F_e = 1$ and 2; and (c) experimentally observed spectra for the resonant transitions of $F_g = 2 \rightarrow F_e = 1$, $F_g = 2 \rightarrow F_e = 2$ and $F_g = 2 \rightarrow F_e = 3$.

A relatively strong EIA amplitude with a narrow linewidth resolution of 58 kHz at the $F_g = 2 \rightarrow F_e = 3$ closed transition and weak EITs with linewidths of 57 kHz and 73 kHz at $F_g = 2 \rightarrow F_e = 1$ and $F_g = 2 \rightarrow F_e = 2$ open transitions, respectively, were obtained, using a DTLS calculation as shown in Fig. 3(a). Here, the linewidth is defined as the full-width at the half maximum (FWHM). However, the spectra obtained considering all the neighboring transitions and experiments showed a striking similarity in the trends presented in Figs. 3(b) and 3(c). The EIT at the $F_g = 2 \rightarrow F_e = 1$ open transition and EIAs at the $F_g = 2 \rightarrow F_e = 2$ open and $F_g = 2 \rightarrow F_e = 3$ closed transitions were resolved with linewidths of 69 kHz, 47 kHz, and 54 kHz (91 kHz, 41 kHz, and 117 kHz), respectively, considering all the neighboring transitions calculations (experiments). We note that there are substantial deviations in the linewidths between the experimental and theoretical spectra. The discrepancy may result from the effect of the ambient magnetic field, imperfect alignment of coupling and probe laser beams, and other effects that are not included in the calculation of the spectra.

The strong EIA amplitude owing to the same polarization between the coupling and probe fields resulted from a transfer of population [20], producing a coherence between the same magnetic sublevels at the $F_g = 2 \rightarrow F_e = 3$ closed transition, which dominated the nearby neighboring $F_g = 2 \rightarrow F_e = 2$ open transition to transform into EIA, as shown in the middle traces of Figs. 3(b) and 3(c). However, the $F_g = 2 \rightarrow F_e = 1$ open transition was strongly influenced by the near neighboring $F_g = 2 \rightarrow F_e = 2$ open transition, which resulted in relatively strong amplitudes of EIT, as shown in the bottom traces of Figs. 3(b) and 3(c) compared to the amplitudes obtained considering DTLS, as indicated in the bottom trace of Fig. 3(a).

A comparison of the simulated and observed spectra of the ^{85}Rb D2 line with the same circular polarization of the coupling and probe fields is shown in Fig. 4 considering (a) DTLS with resonant transitions of $F_g = 3 \rightarrow F_e = 2$, $F_g = 3 \rightarrow F_e = 3$, and $F_g = 3 \rightarrow F_e = 4$; (b) resonant transition of $F_g = 3 \rightarrow F_e = 2$ with neighboring hyperfine transitions of $F_g = 3 \rightarrow F_e = 3$ and 4, resonant transition of $F_g = 3 \rightarrow F_e = 3$ with neighboring transitions of $F_g = 3 \rightarrow F_e = 2$ and 4, resonant transition of $F_g = 3 \rightarrow F_e = 4$ with neighboring transitions of $F_g = 3 \rightarrow F_e = 2$ and 3; and (c) experimentally observed spectra for the resonant transitions of $F_g = 3 \rightarrow F_e = 2$, $F_g = 3 \rightarrow F_e = 3$, and $F_g = 3 \rightarrow F_e = 4$.

For the DTLS simulation shown in Fig. 4(a), strong amplitude EIA dip with a 59 kHz linewidth at the $F_g = 3 \rightarrow F_e = 4$ transition and EITs with 79 kHz and 69 kHz linewidths at the $F_g = 3 \rightarrow F_e = 2$ and $F_g = 3 \rightarrow F_e = 3$ transitions, respectively, were well resolved as expected. Spectral features at the $F_g = 3 \rightarrow F_e = 2$, $F_g = 3 \rightarrow F_e = 3$, and $F_g = 3 \rightarrow F_e = 4$ transitions of ^{85}Rb D2 line exhibited similar trends to

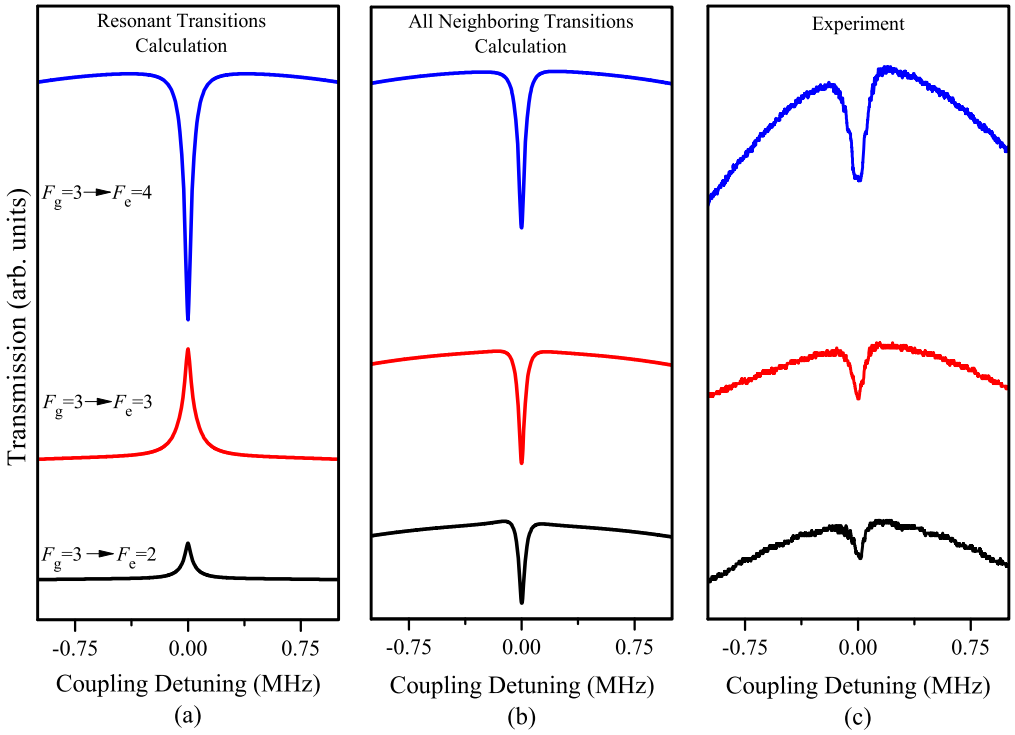

Fig. 4. Comparison of simulated and observed spectra at $F_g = 3 \rightarrow F_e = 2$, 3, and 4 of ^{85}Rb D2 line considering (a) DTLS with resonant transitions of only $F_g = 3 \rightarrow F_e = 2$, $F_g = 3 \rightarrow F_e = 3$, and $F_g = 3 \rightarrow F_e = 4$ shown vertically in (a); (b) all neighboring hyperfine transitions near the resonant (neighboring) transitions of $F_g = 3 \rightarrow F_e = 2$ (3 and 4), $F_g = 3 \rightarrow F_e = 3$ (2 and 4), and $F_g = 3 \rightarrow F_e = 4$ (2 and 3); and (c) experimentally observed spectra for the resonant transitions of $F_g = 3 \rightarrow F_e = 2$, $F_g = 3 \rightarrow F_e = 3$, and $F_g = 3 \rightarrow F_e = 4$.

those simulated for the ^{87}Rb D2 line presented in Fig. 3(a). However, compared to the spectra obtained for the ^{87}Rb D2 line, the simulations considering all the neighboring states and experiments showed EIAs at all the resonant transitions of $F_g = 3 \rightarrow F_e = 2$, $F_g = 3 \rightarrow F_e = 3$, and $F_g = 3 \rightarrow F_e = 4$ of ^{85}Rb atoms owing to strong Doppler overlapping between excited states hyperfine levels, as indicated in Figs. 4(b) and (c). EIAs were resolved with 49 kHz, 49 kHz, and 50 kHz (62 kHz, 85 kHz, and 137 kHz) linewidths, considering all neighboring state simulations (experiments) at the $F_g = 3 \rightarrow F_e = 2$, $F_g = 3 \rightarrow F_e = 3$, and $F_g = 3 \rightarrow F_e = 4$ transitions, respectively.

To understand the opposite behavior of the coherent resonances for the $F_g = 2 \rightarrow F_e = 1$ transition in ^{87}Rb and the $F_g = 3 \rightarrow F_e = 2$ transition in ^{85}Rb shown in Figs. 3(c) and 4(c), respectively, we simulated spectral variations for the $F_g = 3 \rightarrow F_e = 2$ transition in ^{85}Rb by varying the hyperfine splittings of ^{85}Rb artificially. The results are presented in Fig. 5. The ratio in Fig. 5 implies the artificial enhancement factor of the hyperfine splittings of ^{85}Rb. We note that a factor of 2.3 approximately corresponds to the hyperfine splittings of ^{87}Rb. The trace at the unity ratio in Fig. 5, exhibiting EIA, is identical to that in the lowest panel of Fig. 4(b). As the ratio increases, the spectral lineshape changes and the EIA is transformed to EIT at a ratio approximately between 1.5 and 1.8. When a ratio is 2.3 corresponding to ^{87}Rb hyperfine splitting, we observe EIA as shown in Fig. 3(b). We note that there exist no significant differences between the spectra of the ^{87}Rb and ^{85}Rb atoms as long as the hyperfine splittings are artificially set to similar values. In Fig. 5, we can clearly see that the opposite behavior of the resonances for the $F_g = 2 \rightarrow F_e = 1$ transition in ^{87}Rb and the $F_g = 3 \rightarrow F_e = 2$ transition in ^{85}Rb results from the weak influence of the $F_g = 2 \rightarrow F_e = 3$ transition in ^{87}Rb owing to the relatively large hyperfine splitting compared to ^{85}Rb. Qualitatively, as the hyperfine splitting increases, the neighboring effects come from the atoms with higher velocities. Accordingly, the effect on EIA and EIT spectra from neighboring transition is weakened.

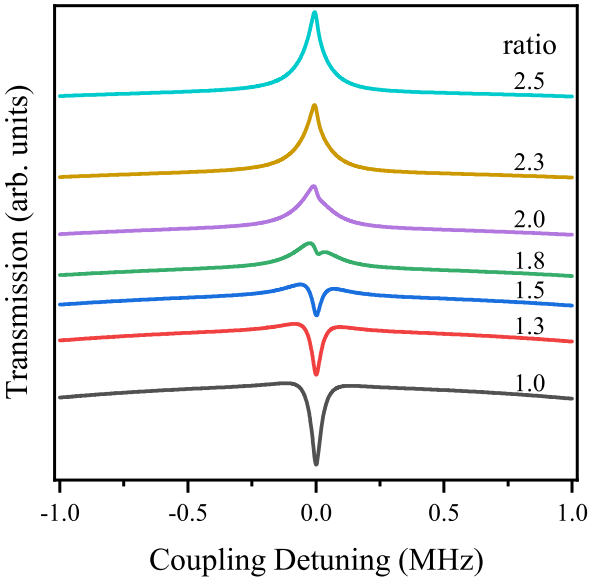

Fig. 5. Spectral variations with respect to the artificial variation in the hyperfine splittings of ^{85}Rb. The unity ratio corresponds to the hyperfine splitting of ^{85}Rb and a ratio of 2.3 corresponds to ^{87}Rb hyperfine splitting.

5. Conclusions

In this work, EIA and EIT at the $F_g = 2 \rightarrow F_e = 1$, 2, and 3 transitions of ^{87}Rb and $F_g = 3 \rightarrow F_e = 2$, 3, and 4 transitions of ^{85}Rb D2 lines were investigated to understand the mechanisms of the neighboring effects with the same circular polarization configurations ($\sigma^+ - \sigma^+$) of coupling and probe lasers. EIA and EIT were observed when $F_g > F_e$ for ^{85}Rb and ^{87}Rb, respectively, for the first time under the same circular

polarization configuration of the coupling and probe beams, although all cases where $F_g \leq F_e$ for both ^{85}Rb and ^{87}Rb exhibited EIAs.

The reason why spectrum remained an EIT for the open $F_g = 2 \rightarrow F_e = 1$ transition of ^{87}Rb in all neighboring transition simulations despite the dominance of EIA was that the DTLS was far away from the dominant EIA transition line; thus, it remained in all neighboring transition simulations as it behaved in DTLS. By contrast, the spectrum for the $F_g = 3 \rightarrow F_e = 2$ transition of ^{85}Rb continued to be EIA in all neighboring transition simulations, because the DTLS was close to the dominant EIA transition line. The opposite behavior of the coherent resonances for the $F_g = 2 \rightarrow F_e = 1$ transition in ^{87}Rb and the $F_g = 3 \rightarrow F_e = 2$ transition in ^{85}Rb was confirmed by calculating the spectral variations for the $F_g = 3 \rightarrow F_e = 2$ transition in ^{85}Rb by varying the hyperfine splittings of ^{85}Rb artificially.

Declarations

Author contribution statement

Zeeshan Ali Safdar Jadoon: Conceived and designed the experiments; Performed the experiments; Analyzed and interpreted the data; Wrote the paper. Aisar Ul Hassan: Performed the experiments. Heung-Ryoul Noh & Jin-Tae Kim: Conceived and designed the experiments; Analyzed and interpreted the data; Wrote the paper.

Funding statement

Jin-Tae Kim was supported by National Science Foundation of Korea [2021r1f1a1052487], Chosun University [2021]. Heung-Ryoul Noh was supported by Natural Science Foundation of Korea [20202r1a2c1005499].

Data availability statement

No data was used for the research described in the article.

Declaration of interests statement

The authors declare no conflict of interest.

Additional information

No additional information is available for this paper.

References

[1] C. Andreeva, S. Cartaleva, Y. Dancheva, V. Biancalana, A. Burchianti, C. Marinelli, E. Mariotti, L. Moi, K. Nasyrov, Coherent spectroscopy of degenerate two-level systems in Cs, Phys. Rev. A 66 (2002) 012502.

[2] A.S. Zibrov, A.B. Matsko, Induced absorption resonance on the open $F_g = 1 \rightarrow F_e = 2$ transition of the D1 line of the ^{87}Rb atom, JETP Lett. 82 (2005) 529.

[3] M. Auzinsh, R. Ferber, F. Gahbauer, A. Jarmola, L. Kalvans, Nonlinear magneto-optical resonances at D1 excitation of ^{85}Rb and ^{87}Rb for partially resolved hyperfine F levels, Phys. Rev. A 79 (2009) 053404.

[4] M. Auzinsh, R. Ferber, F. Gahbauer, A. Jarmola, L. Kalvans, F-resolved magneto-optical resonances in the D1 excitation of cesium: experiment and theory, Phys. Rev. A 78 (2008) 013417.

[5] E. Taskova, E. Alipieva, C. Andreeva, D. Brazhnikov, Electromagnetically induced absorption resonances in Hanle-configuration prepared in a paraffin coated ^{87}Rb cell, J. Phys. Conf. Ser. 1492 (2020) 012011.

[6] M. Auzinsh, A. Berzins, R. Ferber, F. Gahbauer, L. Kalvans, A. Mozers, D. Opalevs, Conversion of bright magneto-optical resonances into dark resonances at fixed laser frequency for D2 excitation of atomic rubidium, Phys. Rev. A 85 (2012) 033418.

[7] R.S. Grewal, M. Pattabiraman, Hanle electromagnetically induced absorption in open $F_g \rightarrow F_e \leq F_g$ transitions of the ^{87}Rb D2 line, J. Phys. B, At. Mol. Opt. Phys. 48 (2015) 085501.

[8] H. Ravi, M. Bhattarai, V. Bharti, V. Natarajan, Polarization-dependent tuning of the Hanle effect in the ground state of Cs, Europhys. Lett. 117 (2017) 63002.

[9] Z.A.S. Jadoon, H.R. Noh, J.T. Kim, Multiphoton nonlinear frequency mixing effects on the coherent electromagnetically induced absorption spectra of ^{85}Rb atoms under a longitudinal magnetic field: theory and experiment, Phys. Rev. A 102 (2020) 063714.

[10] Y. Dancheva, G. Alzetta, S. Cartaleva, M. Taslakov, C. Andreeva, Coherent effects on the Zeeman sublevels of hyperfine states in optical pumping of Rb by monomode diode laser, Opt. Commun. 178 (2000) 103.

[11] F. Renzoni, C. Zimmermann, P. Verkerk, E. Arimondo, Enhanced absorption Hanle effect on the $F_g = F \rightarrow F_e = F + 1$ closed transitions, J. Opt. B 3 (2001) S7.

[12] F. Renzoni, S. Cartaleva, G. Alzetta, E. Arimondo, Enhanced absorption Hanle effect in the configuration of crossed laser beam and magnetic field, Phys. Rev. A 63 (2001) 065401.

[13] Z.A.S. Jadoon, H.R. Noh, J.T. Kim, Effects of neighboring transitions on the mechanisms of electromagnetically induced absorption and transparency in an open degenerate multilevel system, Sci. Rep. 12 (2022) 145.

[14] Z.A.S. Jadoon, A.U. Hassan, H.R. Noh, J.T. Kim, Effects of neighboring transitions on electromagnetically induced absorption and transparency in ^{85}Rb atoms based on the linear parallel polarization of coupling and probe beam, Opt. Commun. 520 (2022) 128512.

[15] H.J. Kang, H.R. Noh, Coherence effects in electromagnetically induced transparency in V-type systems of ^{87}Rb, Opt. Express 25 (2017) 21762.

[16] H.R. Noh, S.E. Park, L.Z. Li, J.D. Park, C.H. Cho, Modulation transfer spectroscopy for ^{87}Rb atoms: theory and experiment, Opt. Express 19 (2011) 23444.

[17] G.W. Choi, H.R. Noh, Line shapes in sub-Doppler DAVLL in the ^{87}Rb-D2 line, Opt. Commun. 367 (2016) 312.

[18] G. Moon, S.C. Yang, J.T. Kim, H.R. Noh, Polarization rotation spectral profiles for the D2 line of ^{87}Rb atoms: theory and experiment, J. Phys. B, At. Mol. Opt. Phys. 52 (2019) 225004.

[19] H.U. Rehman, M. Adnan, H.R. Noh, J.T. Kim, Spectral features of electromagnetically induced absorption in ^{85}Rb atoms, J. Phys. B, At. Mol. Opt. Phys. 48 (2015) 115502.

[20] C. Goren, A.D. Wilson-Gordon, M. Rosenbluh, H. Friedmann, Electromagnetically induced absorption due to transfer of population in degenerate two-level systems, Phys. Rev. A 70 (2004) 043814.